magnetochemistry

MDPI

Article

Effects of Perpendicular Magnetic Field Annealing on the Structural and Magnetic Properties of $[Co/Ni]_2/PtMn$ Thin Films

Roshni Yadav [1], Chun-Hsien Wu [1], I-Fen Huang [1], Xu Li [2,*], Te-Ho Wu [3] and Ko-Wei Lin [1,*]

[1] Department of Materials Science and Engineering, National Chung Hsing University, Taichung 402, Taiwan; roshniyadav05@gmail.com (R.Y.); sam_ntust@hotmail.com (C.-H.W.); 2305danny@gmail.com (I-F.H.)
[2] Department of Physics, Xiamen University, Xiamen 361005, China
[3] Graduate School of Materials Science, National Yunlin University of Science and Technology, Yunlin 640, Taiwan; wuth@yuntech.edu.tw
* Correspondence: xuliphys@xmu.edu.cn (X.L.); kwlin@dragon.nchu.edu.tw (K.-W.L.)

Abstract: In this study, $[Co/Ni]_2/PtMn$ thin films with different PtMn thicknesses (2.7 to 32.4 nm) were prepared on Si/SiO_2 substrates. The post-deposition perpendicular magnetic field annealing (MFA) processes were carried out to modify the structures and magnetic properties. The MFA process also induced strong interlayer diffusion, rendering a less sharp interface between Co and Ni and PtMn layers. The transmission electron microscopy (TEM) lattice image analysis has shown that the films consisted of face-centered tetragonal (fct) PtMn (ordered by MFA), body-centered cubic (bcc) NiMn (due to intermixing), in addition to face-centered cubic (fcc) Co, Ni, and PtMn phases. The peak shift (2-theta from 39.9° to 40.3°) in X-ray diffraction spectra also confirmed the structural transition from fcc PtMn to fct PtMn after MFA, in agreement with those obtained by lattice images in TEM. The interdiffusion induced by MFA was also evidenced by the depth profile of X-ray photoelectron spectroscopy (XPS). Further, the magnetic properties measured by vibrating sample magnetometry (VSM) have shown an increased coercivity in MFA-treated samples. This is attributed to the presence of ordered fct PtMn, and NiMn phases exchange coupled to the ferromagnetic $[Co/Ni]_2$ layers. The vertical shift (M_{shift} = −0.03 memu) of the hysteresis loops is ascribed to the pinned spins resulting from perpendicular MFA processes.

Keywords: $[Co/Ni]_2/PtMn$ multilayers; magnetic field annealing; hysteresis loop vertical shift; exchange coupling

Citation: Yadav, R.; Wu, C.-H.; Huang, I-F.; Li, X.; Wu, T.-H.; Lin, K.-W. Effects of Perpendicular Magnetic Field Annealing on the Structural and Magnetic Properties of $[Co/Ni]_2/PtMn$ Thin Films. *Magnetochemistry* **2021**, *7*, 38. https://doi.org/10.3390/magnetochemistry7030038

Academic Editor: Zaher Salman

Received: 31 December 2020
Accepted: 9 March 2021
Published: 12 March 2021

1. Introduction

The discovery of magnetization switching by spin-orbit torques (SOT) has created new opportunities for digital and analog spintronic applications. The antiferromagnet/ferromagnet (AFM/FM) [1] systems engaging heavy metals are promising building blocks for SOT devices because of their enhanced control over the interface [2] and the effects like increased coercivity and shift in the hysteresis loops along the field axis, which was observed in the AFM/FM system [2,3]. The exchange bias field in such a system provides the required effective field for magnetization switching, enabling field-free SOT switching. Unravelling the magnetic properties of such a system is of vital importance for developing SOT devices. Fukami et al. showed the magnetization switching in the absence of applied field in the PtMn (AFM) and Co/Ni (FM) bilayer system with a perpendicular easy axis due to the exchange bias of the AFM [4]. Further, Van DerBrink et al.also reported the switching of the perpendicular magnetization by an in-plane current in the absence of magnetic field in the Pt/Co/IrMn structure [5]. The investigation on the local spin structure at the FM/AFM interface also helps to understand the correlation between the AFM crystalline structure and the amount of magnetization reversal. The coercivity (H_c, the reverse field required to reduce the magnetization to zero [6,7]) of AFM/FM system

was reported to be strongly dependent on the layer structure. Hu et al. showed that the exchange coupling might cause reduced coercivity, depending on the interface coupling and AFM layer thickness. The strong exchange bias but weak coercivity can be obtained depending on the microstructural parameters in FM/AFM bilayer systems [8]. A study in bi-and tri-layered IrMn/NiFe further revealed that the H_c is not only dependent on the thickness of the AFM-layer but also on the alternative order of the layer deposition [9].

PtMn is one of the most extensively used CuAu-I ($L1_0$) type antiferromagnetic materials for the exchange biasing [10,11]. The as-deposited PtMn is non-magnetic with a face-centered cubic (fcc) structure. It transforms into antiferromagnetic with a face-centered tetragonal (fct) structure after annealing at elevated temperatures. The transition from fcc to chemically ordered fct phase after the annealing facilities strong exchange coupling field at the AFM/FM interface [12]. $(Co/Ni)_n$ was proposed to be a prototypical perpendicularly magnetized system [13].Krishnaswamy et al. studied the structure and current-induced switching behavior of the magnetic domains in PtMn/$[Co/Ni]_{1.5}$ and PtMn/$[Co/Ni]_{2.5}$ clarifying the memristive behavior in AFM/FM structures and for further optimization of spin-orbit torque switching [14]. Hence, $(Co/Ni)_n$ multilayers with the heavy metal antiferromagnets have raised great interest because of their strong Dzyaloshinskii-Moriya Interaction (DMI), large SOT and SOT-induced magnetic switching in $(Co/Ni)_n$ [15–18].

In the previous research, the as-deposited PtMn/$[Co/Ni]_2$ multilayers typically possess in-plane magnetic anisotropy [1], which is not a favorable SOT application. MFA [19–21] is an effective methodology for modifying the magnetism of exchange-coupled films [22]. Li et al. reported that the annealed NiO/CoFe thin films show the morphological changes to nanocomposite single layers. The structural and compositional changes result in tailored magnetic properties, increased surface roughness and altered chemical composition, revealing that the MFA process at varied temperatures plays a pivotal role in the magnetism and film compositions [21]. While the SOT switching behavior in the annealed PtMn/[Co/Ni] multilayers was already reported [23], how the annealing process influenced the microstructure and magnetic properties of such a system remain unclear. Vergès et al. studied the spin-orbit torque (SOT) switching in as-deposited and annealed Pt/$[Co/Ni]_2$/PtMn samples. The as-deposited sample shows no exchange bias effect, and the SOT switching is observed under in-plane applied field. However, the annealed sample shows a moderate switching current in a zero magnetic field [24].

In this paper, we have studied the microstructure and magnetic properties of as-deposited and magnetic field annealed (MFA) Ag(8 nm)/[Co(2.5 nm)/Ni(2.3 nm)]$_2$/PtMn(t_{PtMn}) thin films. The correlation between the enhanced exchange coupling and the phase transition after magnetic field annealing provides a new understanding of the magnetism for multilayer PtMn-based ferromagnetic/antiferromagnetic film systems.

2. Results and Discussion

Figure 1a,b shows the 1 × 1 μm^2 surface morphology of as-deposited and magnetic field annealed Ag/$[Co/Ni]_2$/PtMn(t_{PtMn} = 32.4 nm) multilayers characterized by AFM. The film is uniform and possesses a smooth surface. As compared to the as-deposited thin film, the average roughness increases from 1.1 to 1.5 nm after the annealing process. This can be explained by the grain growth, which yields an increase in the surface roughness.

The crystalline structures of as-deposited and annealed Ag/$[Co/Ni]_2$/PtMn(t_{PtMn}) multilayers were characterized by X-ray diffraction (XRD), as shown in Figure 2a. The XRD characterization affirmed the polycrystalline structure of the thin films. Considerable changes were observed for the as-deposited and annealed thin films with the thickest PtMn (t_{PtMn} = 32.4 nm) layer. The diffraction peak at 39.9° (d = 2.25 Å) changed to 40.1° (d = 2.24 Å) after annealing, which corresponds to the phase transition from fcc PtMn (111) to fct PtMn (111). The d-spacing change from 2.25 Å to 2.24 Å verifies the phase transition after annealing [15]. The PtMn (fcc) is likewise seen at a diffraction pinnacle of 46.1° and 67.8°, which corresponds to the (200) and (220) planes. A small peak at 2θ = 44.2°

corresponds to the bcc NiMn (110) phase as shown in Figure 2a, in addition to Co (111) and Ni (111).

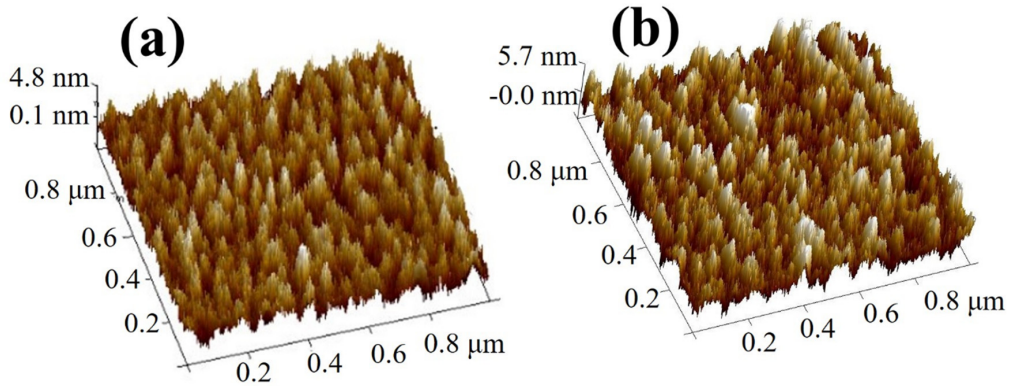

Figure 1. Antiferromagnet (AFM) images of (**a**) as-deposited and (**b**) magnetic field annealing (MFA) samples with a scan area of 1×1 µm^2 Ag/[Co/Ni]$_2$/PtMn(32.4 nm) multilayers.

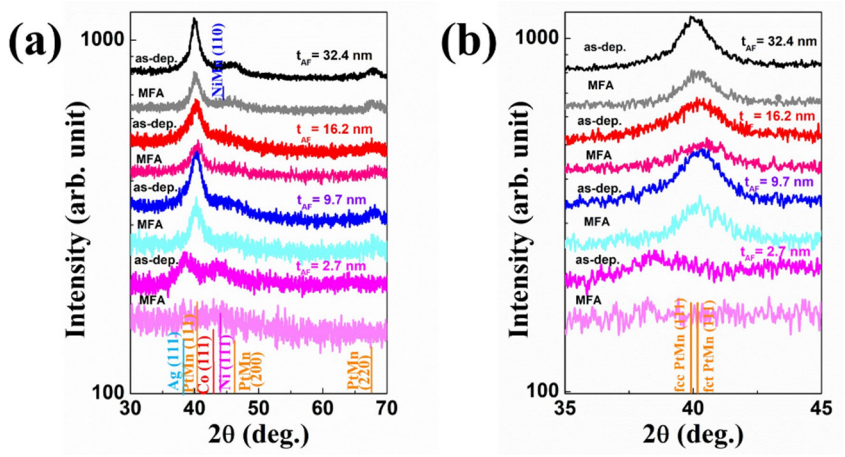

Figure 2. XRD spectra of the as dep. and MFA Ag/[Co/Ni]$_2$/PtMn(t_{PtMn}) multilayered thin films with 2θ from (**a**) 30 to 70 deg. and (**b**) 35 to 45 deg.

Compared with the as-deposited thin film, in the annealed thin film, the phase transformation in the PtMn (t_{PtMn} = 16.2 and 9.7 nm) from fcc (111) to fct (111) was observed where the PtMn (111) peak showed a slight shift of 0.3° from 40° to 40.3°. This shift is evidence of the phase transformation from fcc PtMn (111) to fct PtMn (111) [22]. The broad peak at 2θ = 40.5° (d = 2.22 Å) in samples with t_{PtMn} = 16.2 and 9.7 nm consist of both fcc PtMn (111) and fct PtMn (111) phases as shown in Figure 2b. The observed peak is a superposition of the two individual peaks, which cannot be resolved as they are too closely spaced [11]. During the phase transformation, the decrease in the PtMn (111) peak intensity and the shift to higher peak positions in [Co/Ni]$_2$/PtMn (t_{PtMn} = 16.2 and 9.7 nm) are observed as compared with the [Co/Ni]$_2$/PtMn (t_{PtMn} = 32.4 nm) film. In contrast, no phase transformation with decreasing PtMn thickness is present in the as-deposited samples. The change in intensity during annealing might be due to the fct particles' random orientation [25] or Mn deficiencies within the PtMn film [26]. A weak diffraction peak of fcc PtMn (200) and fct PtMn (220) was also observed. Similar changes were reported by Taras Pokhil et al., where the peak shift from 39.88° to 40.24° was observed, confirming the phase transformation after annealing [27]. In the as-deposited and annealed Ag/[Co/Ni]$_2$/PtMn (t_{PtMn} = 2.7 nm) samples, the thin PtMn layer's diffraction peaks were nearly undetectable possibly due to the small layer thickness.

Further, the elemental mapping along the cross-section of Ag/[Co/Ni]$_2$/PtMn (t_{PtMn} = 2.7 nm) by the Scanning Transmission Electron Microscopy (STEM) is shown in Figure 3. The as-

deposited multilayers exhibited sharp contrast in atomic concentration in Figure 3a. In contrast, the annealed films show strong interdiffusion in Co and Ni interfaces, as evidenced by Co and Ni atoms' broad distribution in Figure 3b.

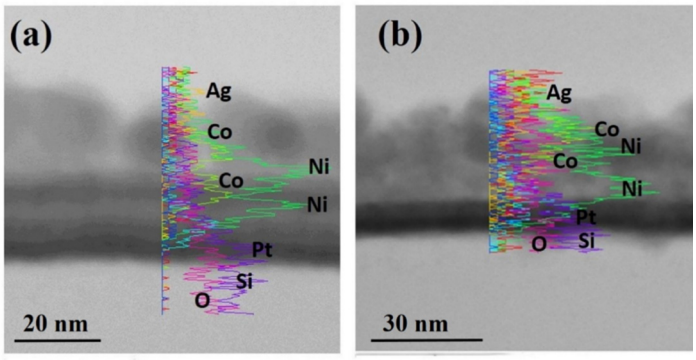

Figure 3. The STEM images and corresponding line scan profiles (**a**) as-deposited and (**b**) MFA Ag/[Co/Ni]$_2$/PtMn(2.7 nm) multilayers.

The high-resolution transmission electron microscopy (HRTEM) image of the annealed Ag/[Co/Ni]$_2$/PtMn multilayers (t_{PtMn} = 2.7 nm) is shown in Figure 4. While this sample exhibits poor XRD signal, the well-crystallized lattices can still be identified from the HRTEM image. A face-centered cubic (111) phase with an interplanar spacing of 0.227 nm was observed in the PtMn layer. The interplanar spacing of 0.222 nm and 0.204 nm were observed in the Ag layer, correlating to the fcc Ag (111) and Ag (200) phases. Similarly, Ni shows the interplanar spacing of 0.206 nm and 0.204 nm corresponding to the Ni (111), whereas the interplanar spacing of 0.204 nm was observed in the Co (111) phase.

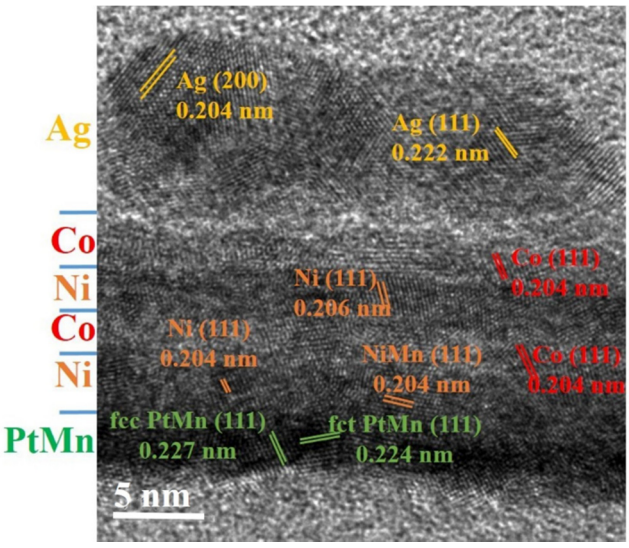

Figure 4. The HRTEM image of Ag/[Co/Ni]$_2$/PtMn(2.7 nm) multilayers after MFA processes.

The annealed Ag/[Co/Ni]$_2$/PtMn multilayers also showed the polycrystalline structures with no sharp interfaces in the multilayer, pointing towards the inter-diffusion between the Ni with the Co and PtMn layers, respectively. The increased crystallinity in the films was observed in each layer after the magnetic field annealing. The lattice spacing of 0.227 nm and 0.224 nm was observed in the PtMn after the annealing, indicating the mixed phases of fcc PtMn (111) and fct PtMn (111) were present in the multilayer thin film consistent with the XRD results. The intermixed bcc NiMn (111) with the interplanar spacing of 0.204 nm was also observed in the Ni layer.

The XPS depth profile observed for as-deposited multilayer is consistent with those obtained by HRTEM, including Ag capping layer, Co, Ni, PtMn layers, and the SiO_2 substrate. The Mn is diffused into the [Co/Ni] layer giving rise to the alloyed NiMn phases. However, Pt remains unreacted with the top Ni (or Co) layers, as shown in Figure 5a. The composition gradient is likely to be present in the film, affecting the respected magnetic properties.

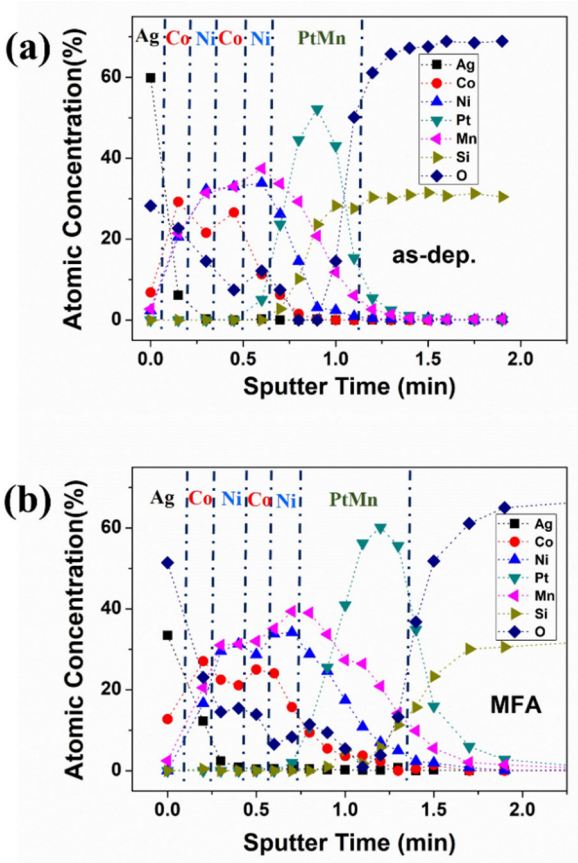

Figure 5. The XPS depth profile of (**a**) the as-deposited and (**b**) the MFA Ag/$[Co/Ni]_2$/PtMn (9.7 nm) multilayers.

Compared to the as-deposited multilayer, a similar layer sequence was observed after the MFA processes. Unlike the as-deposited multilayer, a surface oxide layer was observed by the increased oxygen content in Figure 5b. Diffusion of the Mn into Ni (or Co) layer is observed, indicating the reduction in magnetization contributed from ferromagnetic (FM) $[Co/Ni]_2$ layers.

The XPS spectra of Ag, Co, Ni, Pt, O, and Mn of as-deposited and MFA Ag/$[Co/Ni]_2$/PtMn (9.7 nm) multilayers were shown in Figure 6. The XPS spectra of Ag and O in the Ag capping layer is shown in Figure 6a,b. The binding energy of 367.8 and 373.3 eV in the as-deposited sample corresponds to the Ag $3d_{5/2}$ and Ag $3d_{3/2}$ (Figure 6a). However, after the MFA processes, the peak narrowing and shift towards higher binding energies of 368.2 eV (Ag $3d_{5/2}$) and 374.2 eV (Ag $3d_{3/2}$) indicate the surface oxidization to Ag_2O [28,29]. The Co 2p spectra (778.2 (Co $2P_{3/2}$) and 793.4 eV (Co $2P_{1/2}$)) [30] after the MFA processes (Figure 6c), exhibit a slight shift to higher energies due to the partially oxidized cobalt elements [30]. The O 1s spectra (532.2 eV) confirm the formation of Co-O bonds' in the Co layer (Figure 6d). The Ni 2p spectra (Figure 6e), (852.6 eV (Ni $2P_{3/2}$), 858.6 eV (Ni $2P_{3/2,\,sat.}$), and 870 eV (Ni $2P_{1/2}$)) after the MFA processes exhibit a slight shift to higher energies. This indicates the formation of NiMn alloying phases. The O 1s spectra (529.6 eV), as shown in Figure 6f, indicate the formation of oxides such as Mn oxide due to the diffusion process (Figure 5). The Pt 4f spectra (71.2 eV (Pt $4f_{7/2}$), 74.4 eV (Pt $4f_{5/2}$)) as shown in Figure 6g indicate that Pt was in the metallic state [31,32]. The Mn 2p

spectra (639.8 eV ($2p_{3/2}$), 650.9 eV ($2p_{1/2}$)), (Figure 6h) after MFA processes with a slight shift to higher energies, attribute to the alloy formation [32], i.e., PtMn/NiMn.

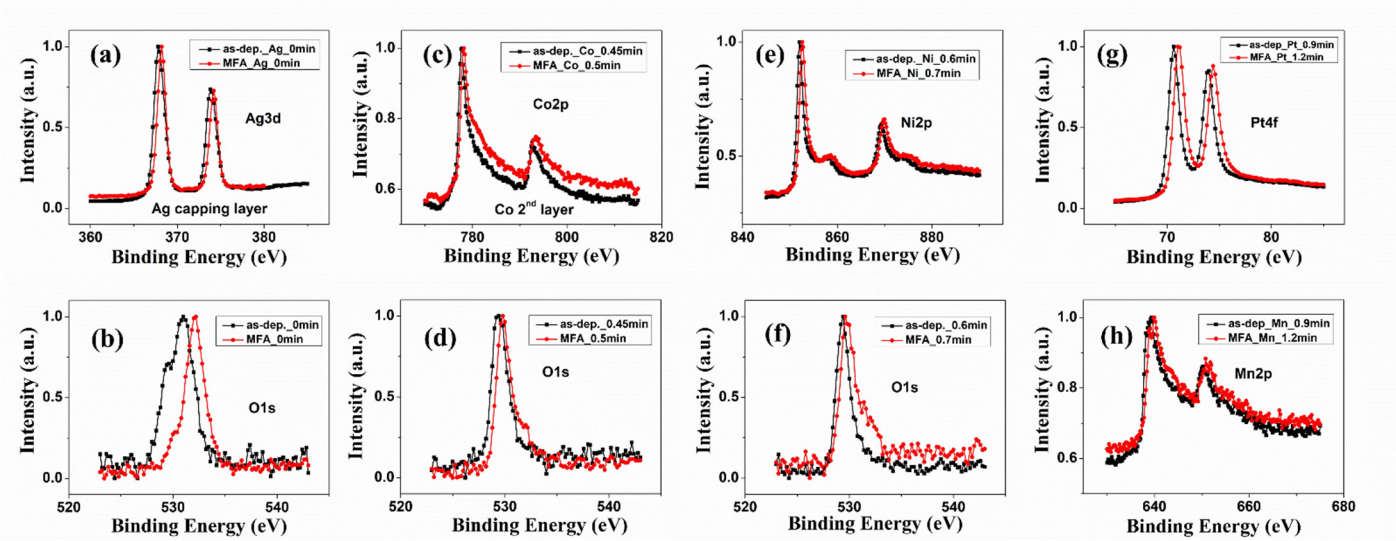

Figure 6. The XPS binding energy spectra of (**a**) Ag 3d, (**b**) O 1s (Ag layer), (**c**) Co 2p, (**d**) O 1s (Co layer), (**e**) Ni 2p, (**f**) O 1s (Ni layer), (**g**) Pt 4f, and (**h**) Mn 2p of the as-deposited and MFA Ag/$[Co/Ni]_2$/PtMn (9.7 nm) multilayers.

To identify the changes in magnetic properties induced by magnetic field annealing, the room temperature in-plane magnetic hysteresis loops of Ag/$[Co/Ni]_2$/PtMn multilayers were shown in Figure 7. As compared with the as-deposited sample, the reduction in the magnetization was seen as a result of the alloying effect between $[Co/Ni]_2$ and PtMn after annealing. The as-deposited and annealed samples of t_{PtMn} = 32.4 nm exhibit the same coercive field of H_c = 20 Oe (Figure 7a). Whereas, with the t_{PtMn} = 16.2 nm, the film shows the coercive field of H_c = 22 Oe in the as-deposited sample and coercive field of about H_c = 28 Oe in the annealed sample (Figure 7b). Similarly, the coercive field of H_c = 24 Oe was observed in the as-deposited sample and H_c = 28 Oe in the annealed sample for the t_{PtMn} = 9.7 nm (Figure 7c).

The vertical shift (m_{shift}) is observed in the annealed sample as compared to the as-deposited sample. The vertical shift along the M-axis is defined as $m_{shift} = \frac{1}{2}(M_{max} + M_{min})$ [33], where the m_{shift} of about −0.03 memu was observed in the sample with t_{PtMn} = 32.4 (Figure 7a). Similarly, m_{shift} of −0.03 memu was observed with the PtMn thickness of 16.2 nm (t_{PtMn}) (Figure 7b) and 9.7 nm (t_{PtMn}) (Figure 7c) respectively, indicating the exchange coupling between FM $[Co/Ni]_2$ and antiferromagnetic (AFM) PtMn layer due to the presence of pinned spins in the samples [33]. The vertical shift observed is due to the pinned moments that do not rotate with the applied field, which defines the bias direction [34].

With the increase in the PtMn thickness, the increased squareness is observed in the as-deposited and annealed samples, as shown in Figure 7d. The maximum squareness (M_r/M_s) observed after annealing is about 0.63, 0.50 and 0.33 with respect to t_{PtMn} = 32.4, 16.2, 9.7 nm as shown in Figure 7d. This can be attributed to the presence of AFM that plays a pivotal role in the enhancement of the M_r/M_s in FM/AFM [33]. With increasing PtMn thickness, the FM layer's magnetization reversal modes switch from domain rotation, pinned by the thin PtMn layer, to spin flipping, which is assisted by the exchange interaction from the thick PtMn layer [35]. The MFA results in higher squareness in samples with a thin PtMn layer, indicating that the MFA acts on the Co/Ni multilayer by repairing structural defects and enhancing magnetocrystalline anisotropy. The reduced squareness in annealed samples with thicker PtMn layer, on the other hand, is attributed to the accelerated interfacial diffusion, which promoted the domain pinning effect. The enhanced coercivity (H_c) of 28 Oe was observed for samples with t_{PtMn} of 9.7 nm and 16.2 nm after annealing because of the ordered fct PtMn during the magnetization reversal processes, as shown in

Figure 7e. As the PtMn layer thickness increases, the decrease in coercivity is observed, which can be explained by the fact that with the increase in PtMn thickness, the effective AFM anisotropy is also increased. The enhanced AFM spins eliminate the amount of reversible interfacial AFM spins, reducing the H_c [2].

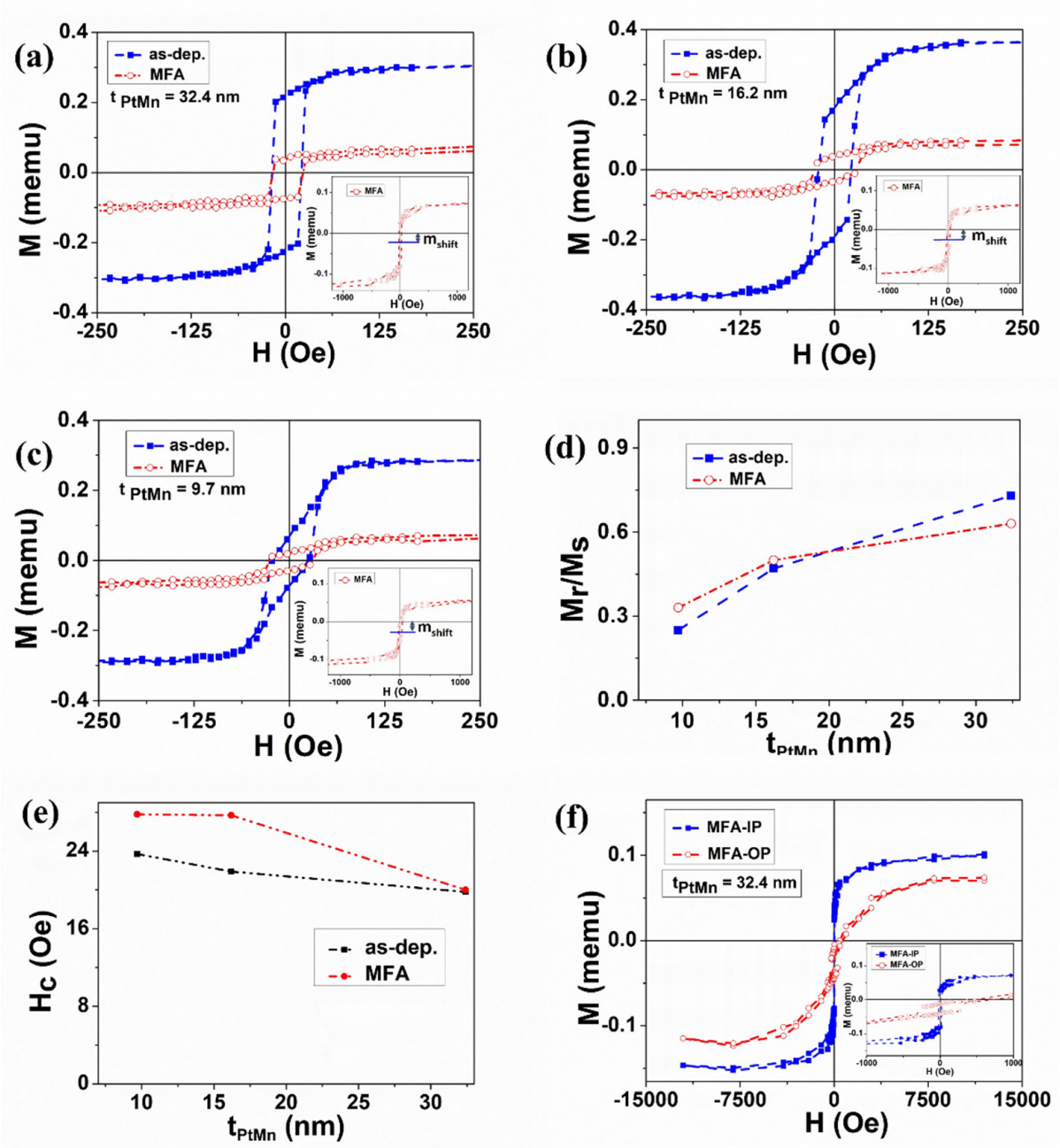

Figure 7. The room temperature in-plane magnetic hysteresis loops of as deposited and MFA Ag/[Co/Ni]$_2$/PtMn (t_{PtMn}) multilayers at (**a**) t_{PtMn} = 32.4 nm, (**b**) t_{PtMn} = 16.2 nm, (**c**) t_{PtMn} = 9.7 nm. The squareness (M_r/M_s) and Coercivity vs. t_{PtMn} is shown in (**d**,**e**), respectively. (**f**) The in-plane and out-of-plane hysteresis loops at t_{PtMn} = 32.4 nm after MFA processes.

The in-plane and out-of-plane hysteresis loop of annealed Ag/[Co/Ni]$_2$/PtMn(32.4 nm) multilayers is shown in Figure 7f. The exchange bias of 2 Oe is observed for the thickest film with a PtMn layer of t_{PtMn} = 32.4 nm. The OP magnetic hysteresis loop show notable hysteretic minor loop in the low field range (Figure 7f inset), indicating the existence of certain perpendicular magnetic anisotropy (PMA). However, this PMA is not strong enough to overcome the perpendicular demagnetization field. The magnetic anisotropy of the multilayer is thus dominated by the IP shape anisotropy, as indicated by the higher

remnant magnetization in the in-plane direction. The out-of-plane and in-plane hysteresis loops are expected to have the same saturation magnetization under "absolute saturation" conditions. However, the measured saturation magnetization usually deviates from the absolute saturation magnetization due to the existence of magnetostriction effects and spin waves [36]. In many cases, the spin-wave spectra are different along different orientations [37]. As a result, the measured saturation magnetizations are not necessarily the same along all directions. In this study, the pinned spins in the in-plane and out-of-plane hysteresis loops (as indicated by the vertical shift in the magnetic hysteresis loops in Figure 7) contributed to the different saturation magnetization in the hysteresis loops. In the sample with PtMn thickness of 32.4 nm, the coercivity (20 Oe) observed is the same for as-deposited and MFA samples; this might be due to the alloyed NiMn dominant over fct PtMn as pinning sites to $[Co/Ni]_2$.

3. Materials and Methods

$[Co(2.5\ nm)/Ni(2.3\ nm)]_2/PtMn(t_{PtMn})$ multilayers [1] were prepared by Ion Beam Assisted Deposition (IBAD) technique [38,39]. $Pt_{69}Mn_{31}$ (at.%) [40] with different thicknesses (t_{PtMn}) of 32.4 nm, 16.2 nm, 9.7 nm, and 2.7 nm were deposited. A Kaufmann ion source operating at 800 V and 7.5 mA was used to subsequently sputter the PtMn, Ni, and Co targets with an argon flow of 3 sccm during the deposition process. The deposition rates for PtMn, Ni, and Co were 3.2, 2.3, and 2.5 nm/min, respectively. The magnetic field annealing (MFA) was conducted at 573 K in a vacuum for 1 h, and a magnetic field of 500 mT was applied perpendicularly to the thin film surface during annealing.

An End-Hall ion source with V_{EH} = 70 V, and I_{EH} = 500 mA was used for bombarding the PtMn layer for 1 min after its deposition. Further, an 8 nm thick Ag capping layer was deposited. The high-resolution lattice image and the line scan profile of the $Ag/[Co/Ni]_2/PtMn$ thin films were obtained using a JEOL-JEM-2100F scanning transmission electron microscopy (STEM) working at 200 kV. The depth profile and binding energy of the $Ag/[Co/Ni]_2/PtMn$ multilayers were characterized by a commercial ULVAC-PHI (PHI 5000 Versa Probe) x-ray photoelectron spectroscopy (XPS). A Veeco D3100 atomic force microscopy (AFM) was utilized to measure the thin multilayer film's surface roughness. The samples' magnetic hysteresis loops were measured by an ADE-DMS 1660 vibrating sample magnetometer (VSM) at room temperature. The saturation magnetization (M_s) is defined as the saturation value at which magnetization (M) becomes constant when a large magnetic field (H) is applied [41]. If the magnetic field (H) is reduced to zero after saturation in the positive direction, the magnetization in the hysteresis loop decreases from M_s to M_r, where M_r is defined as the remnant magnetization [6]. The squareness is defined as the ratio of the remnant magnetization (M_r) to the saturation magnetization (M_s).

4. Conclusions

The microstructure and magnetic properties of as-deposited and MFA $Ag/[Co/Ni]_2/PtMn$ multilayers at different PtMn thickness were investigated. The Co and Ni layers have fcc structures with preferred (111) orientation. The fct PtMn (111) peak intensity increases with PtMn layer thickness in both the as-deposited and MFA samples. After annealing, the phase transformation from fcc (111) to fct (111) is observed in samples with thinner PtMn films (9.7 and 16.2 nm), as was confirmed by XRD and HRTEM. In the STEM, compared to the as-deposited sample, no distinct interface was observed between Co/Ni multilayers due to the inter-diffusion that occurred after the annealing process. The XPS depth profile in MFA $Ag/[Co/Ni]_2/PtMn$ multilayers shows a similar layer sequence as those of the as-deposited sample except for the surface oxide layer. The NiMn alloyed phase formation was also confirmed by the XPS binding energy shift, which results in reduced magnetization.

Further, the magnetic properties measured by VSM show an increased coercivity in the MFA thin films. This is attributed to the presence of ordered fct PtMn, and NiMn phases exchange coupled to the ferromagnetic $[Co/Ni]_2$ layers. No exchange bias field was observed at room temperature. The vertical shift (M_{shift} = −0.03 memu) of the hysteresis loops is

ascribed to the pinned spins resulting from perpendicular MFA processes. The squareness ratio (M_r/M_s) decreases with decreasing PtMn thickness. This work has revealed enhanced coercivity and perpendicular magnetic anisotropy in $[Co/Ni]_2$/PtMn multilayers. The results gain insight into developing perpendicularly magnetized spintronic devices through post-treatment techniques.

Author Contributions: Conceptualization, X.L. and K.-W.L.; data curation, K.-W.L.; formal analysis, R.Y., C.-H.W., I-F.H. and T.-H.W.; funding acquisition, X.L. and K.-W.L.; investigation, T.-H.W.; methodology, X.L. and K.-W.L.; supervision, K.-W.L.; writing—original draft, R.Y.; writing—review and editing, R.Y., X.L. and K.-W.L. All authors have read and agreed to the published version of the manuscript.

Funding: The research was supported by the MOST of Taiwan, the National Natural Science Foundation of China (No. 61804129), and the Science and Technology Project of Fujian Province of China (No. 2019H0002).

Conflicts of Interest: The authors declare no conflict of interest.

References

1. Li, X.; Wu, C.-H.; Lee, Y.-J.; Su, Y.-T.; Lin, K.-W.; Ruotolo, A.; Manna, P.K.; van Lierop, J. Correlating spin freezing and magnetic properties in $[Co/Ni]_n$/PtMn multilayers. *J. Magn. Magn. Mater.* **2020**, *508*, 166690. [CrossRef]
2. Nogués, J.; Schuller, I.K. Exchange bias. *J. Magn. Magn. Mater.* **1999**, *192*, 203. [CrossRef]
3. Meiklejohn, W.H.; Bean, C.P. New magnetic anisotropy. *Phys. Rev.* **1956**, *102*, 1413. [CrossRef]
4. Fukami, S.; Zhang, C.; Duttagupta, S.; Kurenkov, A.; Ohno, H. Magnetization switching by spin-orbit torque in an antiferromagnet-ferromagnet bilayer system. *Nat. Mater.* **2016**, *15*, 535. [CrossRef] [PubMed]
5. Van DenBrink, A.; Vermijs, G.; Solignac, A.; Koo, J.; Kohlhepp, J.T.; Swagten, H.J.M.; Koopmans, B. Field-free magnetization reversal by spin-Hall effect and exchange bias. *Nat. Commun.* **2016**, *7*, 10854. [CrossRef] [PubMed]
6. Spaldin, A.N. *Magnetic Materials: Fundamentals and Applications*, 2nd ed.; Cambridge University Press: New York, NY, USA, 2010; p. 19.
7. Tang, Y.J.; Roos, B.; Mewes, T.; Demokritov, S.O.; Hillebrands, B.; Wang, Y.J. Enhanced coercivity of exchange-bias Fe/MnPd bilayers. *Appl. Phys. Lett.* **1999**, *75*, 707. [CrossRef]
8. Hu, J.G.; Jin, G.J.; Ma, Y.Q. Thickness dependence of exchange bias and coercivity in a ferromagnetic layer coupled with an antiferromagnetic layer. *J. Appl. Phys.* **2003**, *94*, 2529. [CrossRef]
9. Gritsenko, C.; Dzhun, I.; Babaytsev, G.; Chechenin, N.; Rodionova, V. Exchange Bias and Coercivity Fields as a Function of the Antiferromagnetic Layer Thickness in bi- and tri-layered thin-films Based on IrMn and NiFe. *Phys. Procedia* **2016**, *82*, 51. [CrossRef]
10. Krén, E.; Kádár, G.; Pál, L.; Sólyom, J.; Szabó, P.; Tarnóczi, T. Magnetic structures and exchange interactions in the Mn-Pt system. *Phys. Rev.* **1968**, *171*, 574. [CrossRef]
11. Ladwig, P.F.; Chang, Y.A.; Linville, E.S.; Morrone, A.; Gao, J.; Pant, B.B.; Schlutz, A.E.; Mao, S. Paramagnetic to antiferromagnetic phase transformation in sputter-deposited Pt-Mn thin films. *J. Appl. Phys.* **2003**, *94*, 979. [CrossRef]
12. Lee, C.L.; Kools, J.; Devasahayam, A.J.; Mao, M.; Hu, C.C. Enhancement of exchange bias in thin PtMn antiferromagnets by Ru and Cr nano-lamination. *J. Magn. Magn. Mater.* **2005**, *286*, 200. [CrossRef]
13. He, X.D.; Zhang, L.L.; Wu, G.J.; Gao, J.W.; Ran, P.; Sajjad, M.; Zhou, X.W.; Cao, J.W.; Xi, L.; Zuo, Y.L.; et al. Controllable intrinsic Gilbert damping in Pt buffered [Co/Ni]n multilayers with enhanced perpendicular magnetic anisotropy. *J. Magn. Magn. Mater.* **2021**, *519*, 167429. [CrossRef]
14. Krishnaswamy, G.K.; Kurenkov, A.; Sala, G.; Baumgartner, M.; Krizakova, V.; Nistor, C.; MacCherozzi, F.; Dhesi, S.S.; Fukami, S.; Ohno, H.; et al. Multidomain Memristive Switching of $Pt_{38}Mn_{62}/[Co/Ni]_n$ Multilayers. *Phys. Rev. Appl.* **2020**, *14*, 044036. [CrossRef]
15. Duttagupta, S.; Kurenkov, A.; Tretiakov, O.A.; Krishnaswamy, G.; Sala, G.; Krizakova, V.; Maccherozzi, F.; Dhesi, S.S.; Gambardella, P.; Fukami, S.; et al. Spin-orbit torque switching of an antiferromagnetic metallic heterostructure. *Nat. Commun.* **2020**, *11*, 5715. [CrossRef] [PubMed]
16. DuttaGupta, S.; Kanemura, T.; Zhang, C.; Kurenkov, A.; Fukami, S.; Ohno, H. Spin-orbit torques and Dzyaloshinskii-Moriya interaction in PtMn/[Co/Ni] heterostructures. *Appl. Phys. Lett.* **2017**, *111*, 182412. [CrossRef]
17. Ma, X.; Yu, G.; Razavi, S.A.; Sasaki, S.S.; Li, X.; Hao, K.; Tolbert, S.H.; Wang, K.L.; Li, X. Dzyaloshinskii-Moriya Interaction across an Antiferromagnet-Ferromagnet Interface. *Phys. Rev. Lett.* **2017**, *119*, 027202. [CrossRef]
18. Itoh, R.; Takeuchi, Y.; Duttagupta, S.; Fukami, S.; Ohno, H. Stack structure and temperature dependence of spin-orbit torques in heterostructures with antiferromagnetic PtMn. *Appl. Phys. Lett.* **2019**, *115*, 242404. [CrossRef]
19. Svalov, A.V.; Savin, P.A.; Lepalovskij, V.N.; Larranaga, A.; Vaskovskiy, V.O.; Garcia Arribas, A.; Kurlyandskaya, G.V. Exchange biased FeNi/FeMn bilayers with coercivity and switching field enhanced by FeMn surface oxidation. *AIP Adv.* **2013**, *3*, 092104. [CrossRef]

20. Guo, J.Y.; Tzeng, Y.M.; van Lierop, J.; Chang, S.-Y.; Lin, K.-W. Thermal annealing effects on the structural, magnetic, and magnetotransport properties of NiFe/(Ni, Fe)O bilayers. *Jpn. J. Appl. Phys.* **2009**, *48*, 073003. [CrossRef]
21. Li, X.; Chang, Y.-C.; Chen, J.-Y.; Lin, K.-W.; Desautels, R.D.; van Lierop, J.; Pong, P.W.T. Annealing effect of $NiO/Co_{90}Fe_{10}$ thin films: From bilayer to nanocomposite. *Phys. Lett. A* **2018**, *382*, 2886. [CrossRef]
22. Xu, M.; Lu, Z.; Yang, T.; Liu, C.; Cui, S.; Mai, Z.; Lai, W. Relation between microstructures and magnetic properties upon annealing in $Fe_{50}Mn_{50}/Ni_{80}Fe_{20}$ films. *J. Appl. Phys.* **2002**, *92*, 2052. [CrossRef]
23. Kurenkov, A.; Zhang, C.; DuttaGupta, S.; Fukami, S.; Ohno, H. Device-size dependence of field-free spin-orbit torque induced magnetization switching in antiferromagnet/ferromagnet structures. *Appl. Phys. Lett.* **2017**, *110*, 092410. [CrossRef]
24. Vergès, M.; Kumar, V.; Lin, P.H.; Mangin, S.; Lai, C.H. Role of induced exchange bias in zero field spin-orbit torque magnetization switching in Pt/[Ni/Co]/PtMn. *AIP Adv.* **2020**, *10*, 085320. [CrossRef]
25. Soeya, S. Enhanced exchange anisotropy between antiferromagnetic PtMn and ferromagnetic Co system by AuCu underlayer. *Appl. Phys. Lett.* **2009**, *94*, 242507. [CrossRef]
26. An, Y.; Liu, J.; Ma, Y.; Wu, Z. Effect of grain size on the properties of NiFe/PtMn bilayers. *J. Phys. D Appl. Phys.* **2008**, *41*, 165003. [CrossRef]
27. Pokhil, T.; Linville, E.; Mao, S. Exchange anisotropy and micromagnetic properties of PtMn/NiFe bilayers. *J. Appl. Phys.* **2001**, *89*, 6588. [CrossRef]
28. Kaushik, V.K. XPS core level spectra and Auger parameters for some silver compounds. *J. Electron Spectros. Relat. Phenom.* **1991**, *56*, 273. [CrossRef]
29. Vasil'kov, A.Y.; Dovnar, R.I.; Smotryn, S.M.; Iaskevich, N.N.; Naumkin, A.V. Plasmon resonance of silver nanoparticles as a method of increasing their antibacterial action. *Antibiotics* **2018**, *7*, 80. [CrossRef]
30. Lin, K.W.; Lin, F.T.; Tzeng, Y.M. X-ray photoelectron spectroscopy and magnetic force microscopy studies of ion-beam deposited $Ni_{80}Fe_{20}$/Co-oxide bilayers. *IEEE Trans. Magn.* **2005**, *41*, 927. [CrossRef]
31. Shyu, J.Z.; Otto, K. Identification of platinum phases on γ-alumina by XPS. *Appl. Surf. Sci.* **1988**, *32*, 246. [CrossRef]
32. Hu, J.; Fang, C.; Jiang, X.; Zhang, D.; Cui, Z. PtMn/PtCo alloy nanofascicles: Robust electrocatalysts for electrocatalytic hydrogen evolution reaction under both acidic and alkaline conditions. *Inorg. Chem. Front.* **2020**, *7*, 4377. [CrossRef]
33. De La Venta, J.; Erekhinsky, M.; Wang, S.; West, K.G.; Morales, R.; Schuller, I.K. Exchange bias induced by the Fe_3O_4 Verwey transition. *Phys. Rev. B* **2012**, *85*, 13447. [CrossRef]
34. Ohldag, H.; Scholl, A.; Nolting, F.; Arenholz, E.; Maat, S.; Young, A.T.; Carey, M.; Stohr, J. Correlation between Exchange Bias and Pinned Interfacial Spins. *Phys. Rev. Lett.* **2003**, *91*, 017203. [CrossRef]
35. Sort, J.; Nogués, J.; Suriñach, S.; Muñoz, J.S.; Baró, M.D.; Chappel, E.; Dupont, F.; Chouteau, G. Coercivity and squareness enhancement in ball-milled hard magnetic-antiferromagnetic composites. *Appl. Phys. Lett.* **2001**, *79*, 1142. [CrossRef]
36. Kronmüller, H.; Grimm, H. High-field susceptibility and the spin-wave spectrum of $Fe_{40}Ni_{40}P_{14}B_6$-alloys. *J. Magn. Magn. Mater.* **1977**, *6*, 57. [CrossRef]
37. Mook, H.A.; Nicklow, R.M.; Thompson, E.D.; Wilkinson, M.K. Spin-Wave Spectrum of Nickel Metal. *J. Appl. Phys.* **1969**, *40*, 1450. [CrossRef]
38. Lin, K.W.; Chen, T.-J.; Guo, J.-Y.; Ouyang, H.; Wei, D.-H.; van Lierop, J. Correlating antiferromagnetic spin structures with ion-beam bombardment in exchange-biased NiFe/Mn bilayers. *J. Appl. Phys.* **2009**, *105*, 07D710. [CrossRef]
39. Lin, K.W.; Ouyang, C.H.; van Lierop, J. *Using Ion-Beam-Assisted Deposition and Ion Implantation for the Rational Control of Nanomagnetism in Thin Film and Nanostructured Systems*, 1st ed.; Camley, R.E., Stamps, R.L., Eds.; Solid State Physics; Elsevier Academic Press: London, UK, 2018; Volume 69, pp. 1–45.
40. Yadav, R.; Shepit, M.; Li, X.; Lin, K.-W.; van Lierop, J.; Ruotolo, A. Photo-spin-voltaic effect in $PtMn/Y_3Fe_5O_{12}$ thin films. *J. Phys. Condens. Matter* **2021**, *33*, 095802. [CrossRef]
41. Cullity, B.D.; Graham, C.D. *Introduction to Magnetic Materials*, 2nd ed.; John Wiley & Sons: Hoboken, NJ, USA, 2009; p. 14.